Small form factor implantable neural probe with efficient flip chip µLED for in vivo optogenetics

Mafalda Abrantes[1,2,3,*], Tiago Pereira[1,2,*], Patrícia Silva[1], Margarida Falcão[1], Jérôme Borme[2], Pedro Alpuim[2,3], Luis Jacinto[1,†]

[1] Department of Biomedicine – Experimental Biology Unit, Faculty of Medicine, University of Porto (FMUP), 4200-319, Porto, Portugal
[2] International Iberian Nanotechnology Laboratory, 4715-330, Braga, Portugal
[3] Centro de Física das Universidades do Minho e Porto, Universidade do Minho, 4710-057, Braga, Portugal

* These authors contributed equally

[†] Department of Biomedicine – Experimental Biology Unit, Faculty of Medicine of the University of Porto (FMUP), 4200-319, Porto, Portugal
Email addresses: ljacinto@med.up.pt (L. Jacinto)

Abstract

Optogenetics is a widely used tool to dissect neural circuits with optical stimulation, but it requires that light is delivered to photosensitive neurons inside the brain. Implantable neural probes with microscale LEDs (µLEDs) are an emerging approach to delivering light to the brain with superior light output control. However, approaches to integrate µLEDs in neural probes depend on complex fabrication processes. Here, we developed an implantable small form factor neural probe that integrates highly efficient commercial flip chip µLEDs using only standard lithography processes in silicon and a custom automated LED mounting approach with custom 3D-printed tools on a pick-and-place machine. The probe has a cross-sectional area under 0.013 mm^2 but can output up to 2.3 mW of optical power with an irradiance of 175 mW/mm^2. Due to the high plug efficiency of the LED and wide large interconnect lines, the neural probe has improved heat dissipation properties and can perform stimulation protocols up to 50 Hz and 90% duty cycles without surpassing hotspot temperature elevations above 1 ºC. The neural probes were validated in vivo, with brain activity in the motor cortex of transgenic optogenetic mice being reliably modulated by pulsed light emitted from the probe.

Keywords: µLED, flip chip, silicon, neural probe, optogenetics, optoelectronics

1. Introduction

Optogenetics is a powerful tool to modulate neuronal circuits with optical stimulation, and it has been widely used to dissect functional connections in the brains of preclinical animal models [1]–[3]. Through the genetic modification of neuronal cells under the control of specific promoters to express light-gated channels and pumps, optogenetics allows selective excitation and inhibition of neuronal circuits with millisecond resolution using different light wavelengths [4], [5]. This has allowed researchers to map functional connections between different cell types in brain circuits or between different brain areas, as well as to highlight potential cellular targets for brain disorders [3], [6], [7]. Initial approaches to deliver light inside the brain to activate photosensitive cells resorted to optical fibers connected to an external light source such as a laser or an LED [8]. These systems were widely disseminated as they are easily scalable, and optical fiber implants are simple to fabricate. Over the past decade, advances in optoelectronics, photonics, and microfabrication processes led to alternative approaches in which the light source could be implanted inside the brain. [9]–[11], for example, by the integration of microscale LEDs (µLEDs) in micron-size implantable neural probes using silicon-based MEMS fabrication techniques similar to the ones already used for developing neural probes for electrophysiological recordings [9], [12]. Neural probes with µLEDs allow direct light output control with low operational currents and voltages, facilitating multiplexed array designs and wireless operation [12].

The integration of µLEDs in neural probes for optogenetics can follow different routes, each with advantages and disadvantages. One route resorts to monolithic integration by fabricating the device directly on sapphire or silicon epitaxial wafers with gallium nitride (GaN) [13]–[15]. This option offers limited substrate choices and can bring additional compromises regarding materials and processes [9], [16]. Because the entire wafer is used for device fabrication, a thinning step is often necessary to reduce the probe's final implant footprint [13], [15]. Another route consists of epitaxial lift-off followed by transfer printing to a target substrate such as silicon [17] or polyimide [18], [19]. This approach retains the optoelectronic performance of µLEDs grown on the epitaxial wafers and introduces fabrication flexibility of the final device, including in the choice of substrates that can then be released to create smaller cross-section or flexible neural probes [18], [19]. However, the transfer and bonding steps can be complex, requiring temporary handling wafers or assistive transfer support materials and post-transfer processing steps. Both routes can produce very thin µLEDs (< 5 µm) integrated into reduced thickness neural probes (15-120 µm) but typically suffer from low wall-plug efficiency (< 1-2%) and low optical power and irradiance.

An alternative route is the integration of commercially available small-footprint flip chip µLEDs, that were produced for other applications, through micrometric positioning and bonding to appropriate bonding pads fabricated on the probe's substrate. But, placing and effectively bonding and passivating the chips can be challenging due to their small size and the reduced dimensions

of the implantable shanks in the neural probes. Previous approaches have mainly used large area µLEDs (> 0.06 mm^2) and thicker substrates (up to 700 µm) that can withstand the post-fabrication mounting and bonding processes to overcome such difficulties [20]–[23]. The result is neural probes with large cross-sectional areas, potentially leading to more tissue damage upon implantation and poor performance.

In addition to the implant footprint, another concern with implantable neural probes with µLEDs is that a large portion of the input power is converted into heat, not optical power [24]. Temperature elevations in brain tissue can have modulatory effects on neuronal cell activity or even cause tissue damage [1], [24], [25]. Although there are no official guidelines, there is acceptance that µLEDs should not increase brain temperature by more than 1 ºC during operation [24]. Due to the low wall-plug efficiency of µLEDs used in neural probes and the necessity of using higher voltages to achieve reliable turn-on currents, most neural probes with µLEDs are limited to either low driving currents or low frequency and duty-cycle stimulation protocols to avoid unintended temperature elevations above the 1 ºC limit.

Here, we report on an implantable silicon-based neural probe that integrates highly efficient small-sized commercial bare die µLEDs on thin shanks with a small final cross-section, high optical output power, and outstanding heat dissipation. A custom method was developed to mount, bond, and passivate the µLEDs on 15 µm-thin probe shanks using custom-printed 3D tools on a pick-and-place machine. The final cross-sectional area of the probe is only 0.013 mm^2, which is significantly smaller than that of the smallest optical fiber implants used in mice. The probe can output up to 2.3 mW of optical power with an irradiance of 175 mW/mm^2, with approximately 15% plug-efficiency while maintaining hotspot temperature elevation below 1 ºC for frequencies up to 50 Hz and duty cycles below 90%. The probe was validated in vivo by reliably driving opto-evoked activity in the motor cortex of transgenic mice.

2. Methods

2.1 Neural probe fabrication

A standard silicon-on-insulator (SOI) wafer (15 µm silicon (Si) / 2 µm silicon dioxide (SiO_2) / 650 µm Si / 2 µm SiO_2) (Silicon Valley Microelectronics) was used (Figure 1a). The fabrication process started with the sputtering of an alumina insulator film (Al_2O_3, 100 nm) on the front side of the wafer, and the deposition of 1500 nm of SiO_2 on the back side by plasma-enhanced chemical vapor deposition (PECVD) (Figure 1b,c). Then, a 5 nm layer of chromium (Cr), as adhesion for the gold (Au) contact layer, and 200 nm of Au were sputtered on the front side (Figure 1d). Probe contacts, pads, and conductive lines were patterned by photolithography and

etched by ion beam (Figure 1e,f). On the back side, a SiO_2 hard mask was patterned by reactive ion etching to define the regions that would later be etched up to the device layer (Figure 1g,h). A layer of 200 nm of Al_2O_3 was deposited on the front side by atomic layer deposition (ALD) for device passivation, and probe contacts and pads were exposed by ion milling (Figure 1i,j,k). The outline of each probe was defined by photolithography, and the wafer's Si device layer (15 µm) was etched by deep reactive ion etching (DRIE) (Figure 1l.m). Then, the back side of the wafer (Si 650 µm) was etched with the same DRIE process until the buried 2 µm SiO_2-layer was reached (Figure 1n). Finally, the buried oxide layer of the neural probe shank was etched by hydrogen fluoride (HF) vapor (Figure 1o,p). Probes were released from the wafer by breaking two thin silicon bridges that connected the probes' base to the wafer.

2.2 µLED integration in neural probe

µLEDs (UB06FP2, Light Avenue) were mounted on the neural probe shank by a pick-and-place system (Fineplacer Sigma, Finetech) with custom-designed holders and tips. A specially designed holder for handling the probe during the process was printed on a stereolithography resin 3D printer (Form 3+, Formlabs) and cured by ultra-violet (UV) light exposure (in Form Cure, Formlabs). Double-sided thermal-release tape (TRT) was taped to the holders to attach the probe's shanks. Probes were inserted into the holders with the help of tweezers and, after vacuum fixation in the pick-and-place working stage, these were gently pressed (0.02 N) against the TRT with a custom 3D printed tip tool (with a cylinder tip of 500 µm diameter). Conductive adhesive (Ablestick ABP 8037 TI, Loctite) was stamped on each probe's bonding pad with another stamping tool (150 µm diameter semisphere DAUB tip, Small Precision Tools). Then, the µLEDs were positioned on the pads with a pick-and-place vacuum tool (2-sided Inverted Channel Die Collect, Small Precision Tools) and baked in a furnace to cure the conductive adhesive with a 30 minutes temperature ramp between 25º C and 160 ºC, followed by 45 minutes at 160 ºC. After cooling to room temperature, the µLEDs on the probes' shanks were passivated with a thin 5-10 µm layer of acrylic-based transparent coating for optical applications (8424 UV, IQ-BOND) with a custom pick-and-place 3D printed tool. Finally, the coating was cured with UV-light exposure for 5 s.

2.3 µLED neural probe packaging

The µLED probes were packaged with a custom-designed PCB (5.9 × 6 × 0.8 mm) with electroless nickel immersion gold (ENIG) finishing. Probe connector pads were wire-bonded to

PCB pads with 25 µm gold wire in a wire bonder (HB16, TPT), and a connector (853-93-100-10-001000, Mill-Max Mfg. Corp.) was soldered to the PCB.

2.4 Electrical, optical, and thermal characterization

I-V characterization was performed with a source meter unit (2400 SourceMeter, Keithley) connected to the probe's PCBs with tungsten probes. Voltage sweeps from 2.5 V to 3.2 V were applied with 0.1 V increments, with current limited to 6 mA. Optical output was measured in the same setup by placing a photodiode power sensor (S121C, Thorlabs) above the µLED at approximately 1 mm and connected to a power meter (PM101, Thorlabs). µLED hotspot temperature was measured with a digital infrared temperature sensor (MLX90615, Melexis) connected to an Arduino UNO (rev3, Arduino) for different stimulation frequencies and duty cycles generated by a waveform generator (DG1022z, Rigol). One µLED neural probe was immersed in phosphate-buffered saline (PBS) solution for 12 days, and the current was measured daily to a forward bias of 2.8 V to assess the passivation coating efficiency.

2.5 In vivo testing

A custom tetrode device [26] carrying four nichrome tetrodes was used for electrophysiological recordings. Briefly, tetrodes were prepared by twisting four 12.5 µm nichrome wires (Kanthal) with Twister3 [27] and mounted on the tetrode device with UV-cure epoxy. Following tetrodes connection to the pads with gold pins (Neuralynx), the tips of the tetrodes were cut and gold-plated as in [26]. The µLED neural probe connected to the PCB package was then glued to the tetrode device with UV-cure epoxy so that the µLED was facing the tetrodes' tips at a distance smaller than 1 mm.

One Emx1-Cre:Ai27D male mouse was used for in vivo tests. Mice were obtained by crossing homozygous Emx1-IRES-cre mice with homozygous Ai27D mice (JAX stocks #005628, #012567) [28], [29]. Animals were anesthetized by intraperitoneal injection of ketamine (75 mg/Kg) and medetomidine (1 mg/Kg) mix and securely placed in a stereotaxic frame (World Precision Instruments). The tetrodes and µLED neural probe assembly was lowered into the motor cortex (1.7 mm AP and 1.0 mm ML from bregma) to a depth of at least 0.7 mm (DV) from the brain surface. A stainless-steel screw at the back of the skull served as ground. Extracellular neuronal activity was acquired at 30 kS/s with a headstage (RHD 32ch, Intan) connected to the tetrode device and an Open Ephys acquisition system [30], and filtered between 0.3 and 6 kHz. To evoke neuronal activity from motor cortex neurons expressing channelrhodopsin, the µLED neural probe was powered by a 3 V battery and controlled by an Arduino UNO (rev3, Arduino)

to deliver 0.90 s light stimulation pulses. Each trial had one pulse, and the inter-trial interval was 30 s. The Arduino also sent a 3.3 V TTL pulse during stimulation to the acquisition system for synchronization with the electrophysiological recordings. Evoked electrophysiological responses by optical stimulation were analyzed with custom Python code. Spikes were detected if crossing an amplitude threshold six times higher than the signal standard deviation. Detected spikes were averaged in 200 ms bins for the peristimulus time histogram (PSTH).

3. Results and discussion

3.1 Probe design and fabrication

A small cross-sectional area neural probe with an integrated flip chip µLED that provides high optical power at low driving power was developed in this work for in vivo optogenetics applications. Neural probes were fabricated with standard photolithographic processes on a silicon-on-insulator (SOI) wafer (Figure 2a,b), and the µLED chip was then transferred to the released probes post-fabrication. A SOI wafer was chosen because it allows precise etching of its bottom side to create neural probes with reduced thickness implantable shanks (device layer) and a connector section at full-wafer thickness for safe handling [31], [32]. Probes of 3 and 6 mm lengths were fabricated to allow targeting of different cortical and subcortical brain areas in both rats and mice (Figure 2c). The implantable portion of each probe, regardless of length, consists of a 99 µm wide and 15 µm thick shank with two gold 44 × 33 μm^2 bonding pads with a vertical pitch of 100 µm near the tip for posterior µLED integration (Figure 3d). Both pads are connected to 40 µm wide gold interconnect lines (200 nm thick), with a lateral separation of 7.5 µm, extending to the connector section of the probe. The width of the shank was primarily determined by the width of the µLED to be mounted (89 × 150 µm), and gold interconnect lines were lithographically patterned to occupy most of the available space to reduce line resistance and improve heat dissipation. The connector section of the probe remained at wafer thickness (670 µm) and included two 990 × 490 μm^2 gold contact pads that were used to wire-bond the probe to a custom-designed PCB. The line resistance between µLED bonding pads and connector contact pads was calculated to be 25 and 50 Ω for the 3 and 6 µm length probes, respectively. The width of the interconnect lines could be reduced to include additional µLEDs in the shank, but to retain similar line resistances, the thickness of the deposited gold would have to be increased. The design of probes with multiple shanks to simultaneously target different brain areas could also be realized without changes to the overall fabrication process.

3.2 µLED integration

Integrating bare µLED chips in neural probes allows using highly efficient µLEDs but typically requires thick substrates to withstand the mounting and bonding processes primarily performed post-fabrication. In contrast to previous approaches that led to thick implantable probes [20]–[22], a novel method using custom 3D-printed holders and tips for a pick-and-place system was developed to integrate bare µLED chips with reduced dimensions ($89 \times 150 \times 80$ µm^3) in 15 µm thick suspended silicon neural probe shanks. When compared with other bare µLED chips often used in neural probes, such as the TR2227 ($220 \times 270 \times 50$ µm^3, CREE) [20], [21], [23], the chosen LED for our probes has a considerably smaller footprint albeit being 30 µm thicker. The integration of the µLEDs on the neural probes had to be realized after releasing the probes from the wafer because the LED chips could not withstand the hydrogen fluoride (HF) etch process used to remove the buried oxide layer that released the probe's shanks from the wafer.

Custom 3D-printed holders were designed to hold the released neural probes tightly in position during the µLED bonding process (Figure 3a,b), allowing for an accurate and reproducible process. The 3D printed pieces were designed to have two distinct areas that could accommodate the thickness differences between the probes' shanks (15 µm) and their connector portion (670 µm). Double-sided thermal release tape (TRT) was used in the holders to guarantee that the probe's shank could not move laterally and provide cushioning during the following stamping and bonding procedures (Figure 3b). Different pick-and-place tips, including custom-designed ones, were used to sequentially press the probe's shank against the TRT, stamp conductive glue on the shank's bonding pads, and position and press the µLED on top of the bonding pads (Figure 3c,d,e). Following conductive glue cure in a furnace for 75 mins, where the probes were also released from the TRT, a custom 3D-printed tool was used in the pick-and-place system to passivate the µLED with a thin layer of a UV-cured transparent optical coating (Figure 3f,g). The custom-designed tool creates a coating fluid dome that envelops the µLED and guarantees both the coating of the LED and underfilling between the LED and the neural probe. The tool also allows the final wiping of any excess coating on top of the µLED for a uniform top layer that is only 5-10 µm thick (Figure 3h). The wiping process also extends upward along the shank, away from the µLED, to create a coating slope that reduces the sharp topography change between the shank and the µLED (Figure 3i). This approach is simultaneously more reproducible and more effective in maintaining a reduced probe thickness than, for example, dip coating, which could double the total thickness of the probe [21]. The specific optical coating was chosen because of its optical transparency between 230-500 nm, which encompasses the emission wavelength of the used µLED (465 nm) (Figure 3j), and its reported humidity resistance. To confirm that the optical coating did not reduce the optical output of the µLED, optical power was measured before and after the coating application. An increase in µLEDs optical power after coating was observed

(Figure 3k). It is most likely due to a reduction of the solid angle emission of the LEDs, considering a planar photodetector and not an integrating sphere was used to measure optical power (if using the latter, output power between coated and uncoated LEDs was expected to be similar). The final cross-sectional area of the neural probe, considering the substrate, µLED, and coating, does not exceed 0.013 μm^2, which is not only smaller than in most µLED probes but also smaller than the smallest 100 µm optical fiber implants used in mice implants (having a footprint of approximately 0.050 μm^2 considering the core, cladding, and coating). Table 1 shows a comparison of our neural probe's characteristics with those that have been previously published.

3.3 Electro-optical and thermal characterization

The electrical and optical properties of the fabricated µLED neural probes were evaluated with a source meter and a photodetector on a probe station. Representative I-V curves and radiant flux as a function of current were obtained for the probes with µLEDs (Figure 4a,b,c). Turn-on-voltage was observed at 2.6 V. A maximum optical output power of approximately 2.5 mW and a maximum irradiance of approximately 175 mW/mm^2 was observed at a driving current of 5 mA, which corresponds to approximately 3.2 V of driving voltage (Figure 4b,c). Although some µLEDs on our probes were tested up to 3.5 V and 8 mA with corresponding irradiances of approximately 215 mW/mm^2, others became unstable with currents over 6 mA. Thus, further experimental analysis and probe use were limited to 6 mA. The measured irradiance of 175 mW/mm^2 was significantly higher than those reported for previous µLED-based probes (Table 1) and is well above the threshold of 1 mW/mm^2 necessary for channelrhodopsin activation [33]. The high irradiance in our probes is due to the small emission area of the LED chip (89×150 μm^2) and its high wall-plug efficiency (WPE). The observed WPE of 14.6% is significantly higher than that previously reported for any µLED neural probe (Table 1), allowing our probe to output two orders of magnitude more optical power than previous probes with similar currents (and with many also requiring higher operating voltages) [14], [17], [19], [21], [23], [34].

LEDs are never 100% efficient, and a significant part of the driving power is converted to heat and does not contribute to the optical output [24]. Because many neuronal circuit processes are temperature dependent, it is crucial to assess hotspot temperature elevations in µLED neural probes during optical stimulation with different stimulation parameters typically used in optogenetics experiments [24], [25]. Probe hotspot temperature was measured with an IR thermal sensor at different driving frequencies (10, 20, 30, and 50 Hz) and duty cycles (10-90%) at a maximum operating current of 5 mA (Figure 4d). Although the temperature increased as the duty cycle increased, there were no temperature elevations above 1 ºC for all tested frequencies. Because optogenetic applications typically require pulsed stimulation over time, heat can

accumulate in the neural probe, with peak temperatures for each driving parameter being dependent on the temporal dynamics of heat dissipation in the probe. These dynamics are unknown for most previously proposed µLED neural probes because only average temperatures or temperatures measured at unknown time points have been reported. Here, temperatures were measured at different time points for 10 and 20 Hz stimulation frequencies, often used in optogenetic experiments, at different duty cycles to evaluate heat accumulation in our probe over time (Figure 4e). Regardless of driving parameters, the peak temperature for each condition was reached at approximately 10 seconds after pulsed stimulation started, and the temperature increase never exceeded 1 ºC. This result also means that temperature increases for stimulation durations under 10 seconds will lead to lower heating, as illustrated by the measurements taken after 2 seconds (Figure 4d).

Compared with previously reported µLED neural probes, our probe presents lower heating for similar driving power (Table 1). Although this can be partly explained by the significantly higher WPE of the µLED used, the reduction of the hotspot temperature in our probe may also have occurred due to the combined action of the epoxy encapsulation and the large area of the interconnect lines to block and dissipate heat, respectively. Encapsulation materials, such as the acrylic-based optical coating passivating the µLED, have low thermal conductivity and can block heat transfer. A modeling study determined that µLED hotspot temperatures on neural probes can decrease by 50% with only 20 µm of encapsulation [24]. Heat dissipation can also occur through the substrate [14], [35], with probe shanks working as temporary heat buffers that can prevent hotspot temperature spikes [24]. Although the 15 µm thick shank may have reduced the heat buffer capacity of our probe [24], a large proportion of heat dissipation likely occurred through the interconnect lines due to the high thermal conductivity of gold. Previous reports showed that heat dissipation in µLED probes also occurs through the metal lines and can even lead to considerable hotspot temperature elevations in the exposed electrode sites of probes combining capacitive metal electrodes with µLEDs [15], [24]. The large heat capacity of the brain tissue also prevents significant temperature elevations, and previous studies support that temperature elevations in the tissue will be even lower than those measured at the probe surface [13], [35], [36]. In conclusion, temperature elevations in the brain tissue driven by our neural probe will be significantly below 1 ºC.

3.4 In vivo testing

Before in vivo testing in mice, the longevity of the µLED optical coating encapsulation was assessed. The shank of a neural probe was immersed in phosphate-buffered saline (PBS) continuously for 12 days, and current measurements at 2.8 V were taken every 24h (Figure 5a).

A current of approximately 1.30 mA was measured every day (Figure 5a), confirming that the regular operation of the probe was maintained even in continuous immersion in liquid solution.

A custom tetrode device [26] was combined with a probe for simultaneous optical stimulation and electrophysiological activity recordings to assess the in vivo performance of the µLED neural probe (Figure 5b). One anesthetized Emx1-cre:Ai27D mouse expressing channelrhodopsin in brain cortical neurons was acutely implanted with the tetrodes-µLED probe assembly in the primary motor cortex (M1). Pulsed brain illumination through the µLED at 3 mA reliably induced spiking activity across all trials (Figure 5b). On each trial, the multi-unit activity spike rate increased from below 1 Hz to over 30 Hz, confirming strong neuronal activitation with optical stimulation.

4. Conclusion

In contrast to previous µLED neural probes with monolithically integrated or transfer-printed LEDs with low quantum efficiency and low output power or commercial bare LED chip bonding on thick substrates, we have designed a novel process to integrate low-cost and highly efficient LED chips in neural probes with reduced thickness (15 um). This approach created small form factor implantable neural probes with a cross-section lower than that found in the smallest optical fibers used for in vivo optogenetic studies and with high optical output power with relatively low operating power. Using a commercial µLED with high wall-plug efficiency and designing wide interconnect lines also permitted reducing thermal heating during operation, allowing a wide range of different stimulation frequencies and duty cycles for in vivo optogenetic experiments. In vivo validation with simultaneous electrophysiological recordings confirmed that our neural probe can reliably induce strong spiking activity in neuronal populations expressing channelrhodopsin.

Acknowledgments

The authors would like to thank Helder Fonseca and José Fernandes of INL for assistance with the HF etching process, as well as all members of the Neurophysiology and Neuroengineering Lab at FMUP and the Alpuim group (former 2D Materials and Devices group) at INL for discussions on probe design and fabrication processes.

Author contributions

MA and TP designed the probe layout. MA fabricated the probe, with assistance from JB. TP and JB developed the µLED mounting process. PS designed the interface PCBs and performed probe characterization measurement with TP. MF and PS performed the in vivo tests. PS analyzed electrophysiological recordings. MA, TP, PS, and LJ wrote the first draft of the manuscript. PA and LJ revised the manuscript, acquired funding, and supervised work. All authors read and approved the final version of the manuscript.

Statements and Declarations

Ethics approval: All procedures involving animals were conducted in accordance with European Union Directive 2016/63/EU and the Portuguese law on the protection of animals for scientific purposes (DL No 113/2013), and approved by the Portuguese National Authority for Animal Health and the Animal Welfare Committee at FMUP (ORBEA-FMUP).

Funding: This work was supported by "la Caixa" Banking Foundation under grant agreement LCF/PR/HR21-00410. MA and MF were supported by Portuguese Foundation for Science and Technology (FCT) doctoral fellowships 2022.14536.BD and 2023.00604.BD, respectively.

Competing interests: The authors have no competing interests to declare that are relevant to the content of this article.

References

[1] O. Yizhar, L. E. Fenno, T. J. Davidson, M. Mogri, and K. Deisseroth, "Optogenetics in Neural Systems," *Neuron*. 2011. doi: 10.1016/j.neuron.2011.06.004.

[2] J. G. Bernstein and E. S. Boyden, "Optogenetic tools for analyzing the neural circuits of behavior," *Trends in Cognitive Sciences*. 2011. doi: 10.1016/j.tics.2011.10.003.

[3] K. M. Tye and K. Deisseroth, "Optogenetic investigation of neural circuits underlying brain disease in animal models," *Nature Reviews Neuroscience*. 2012. doi: 10.1038/nrn3171.

[4] L. Fenno, O. Yizhar, and K. Deisseroth, "The development and application of optogenetics," *Annu. Rev. Neurosci.*, 2011, doi: 10.1146/annurev-neuro-061010-113817.

[5] H. Zeng and L. Madisen, "Mouse transgenic approaches in optogenetics," in *Progress in Brain Research*, 2012. doi: 10.1016/B978-0-444-59426-6.00010-0.

[6] W. Chen *et al.*, "The Roles of Optogenetics and Technology in Neurobiology: A Review," *Frontiers in Aging Neuroscience*. 2022. doi: 10.3389/fnagi.2022.867863.

[7] K. Deisseroth, "Circuit dynamics of adaptive and maladaptive behaviour," *Nature*. 2014. doi: 10.1038/nature12982.

[8] M. R. Warden, J. A. Cardin, and K. Deisseroth, "Optical neural interfaces," *Annual Review of Biomedical Engineering*. 2014. doi: 10.1146/annurev-bioeng-071813-104733.

[9] J. Chen, H. Ding, and X. Sheng, "Advanced manufacturing of microscale light-emitting diodes and their use in displays and biomedicine," *J. Inf. Disp.*, 2024, doi: 10.1080/15980316.2023.2248403.

[10] B. J. Barros and J. P. S. Cunha, "Neurophotonics: a comprehensive review, current challenges and future trends," *Front. Neurosci.*, vol. 18, May 2024, doi: 10.3389/fnins.2024.1382341.

[11] S. Xu *et al.*, "Illuminating the Brain: Advances and Perspectives in Optoelectronics for Neural Activity Monitoring and Modulation," *Advanced Materials*. 2023. doi: 10.1002/adma.202303267.

[12] R. Qazi, C. Y. Kim, S. H. Byun, and J. W. Jeong, "Microscale inorganic LED based wireless neural systems for chronic in vivo optogenetics," *Frontiers in Neuroscience*. 2018. doi: 10.3389/fnins.2018.00764.

[13] F. Wu, E. Stark, P. C. Ku, K. D. Wise, G. Buzsáki, and E. Yoon, "Monolithically Integrated μLEDs on Silicon Neural Probes for High-Resolution Optogenetic Studies in

Behaving Animals," *Neuron*, 2015, doi: 10.1016/j.neuron.2015.10.032.

[14] R. Scharf, T. Tsunematsu, N. McAlinden, M. D. Dawson, S. Sakata, and K. Mathieson, "Depth-specific optogenetic control in vivo with a scalable, high-density µlED neural probe," *Sci. Rep.*, 2016, doi: 10.1038/srep28381.

[15] J. W. Reddy *et al.*, "High density, double-sided, flexible optoelectronic neural probes with embedded µLEDs," *Front. Genet.*, vol. 10, no. JUL, 2019, doi: 10.3389/fnins.2019.00745.

[16] S. B. Goncalves, J. F. Ribeiro, A. F. Silva, R. M. Costa, and J. H. Correia, "Design and manufacturing challenges of optogenetic neural interfaces: A review," *Journal of Neural Engineering*. 2017. doi: 10.1088/1741-2552/aa7004.

[17] S. Ayub *et al.*, "Compact Optical Neural Probes with up to 20 Integrated Thin-Film LEDs Applied in Acute Optogenetic Studies," *IEEE Trans. Biomed. Eng.*, 2020, doi: 10.1109/TBME.2020.2966293.

[18] T. Il Kim *et al.*, "Injectable, cellular-scale optoelectronics with applications for wireless optogenetics," *Science (80-.).*, 2013, doi: 10.1126/science.1232437.

[19] L. Li *et al.*, "Colocalized, bidirectional optogenetic modulations in freely behaving mice with a wireless dual-color optoelectronic probe," *Nat. Commun.*, 2022, doi: 10.1038/s41467-022-28539-7.

[20] S. Il Park *et al.*, "Stretchable multichannel antennas in soft wireless optoelectronic implants for optogenetics," *Proc. Natl. Acad. Sci. U. S. A.*, 2016, doi: 10.1073/pnas.1611769113.

[21] G. Shin *et al.*, "Flexible Near-Field Wireless Optoelectronics as Subdermal Implants for Broad Applications in Optogenetics," *Neuron*, 2017, doi: 10.1016/j.neuron.2016.12.031.

[22] B. Fan, K.-Y. Kwon, R. Rechenberg, M. F. Becker, A. J. Weber, and W. Li, "A hybrid neural interface optrode with a polycrystalline diamond heat spreader for optogenetics," *TECHNOLOGY*, 2016, doi: 10.1142/s2339547816400021.

[23] S. Ayub *et al.*, "Hybrid intracerebral probe with integrated bare LED chips for optogenetic studies," *Biomed. Microdevices*, 2017, doi: 10.1007/s10544-017-0190-3.

[24] N. Dong *et al.*, "Opto-electro-thermal optimization of photonic probes for optogenetic neural stimulation," *J. Biophotonics*, 2018, doi: 10.1002/jbio.201700358.

[25] S. F. Owen, M. H. Liu, and A. C. Kreitzer, "Thermal constraints on in vivo optogenetic manipulations," *Nat. Neurosci.*, 2019, doi: 10.1038/s41593-019-0422-3.

[26] F. Machado, N. Sousa, P. Monteiro, and L. Jacinto, “A versatile and modular tetrode-based device for single-unit recordings in rodent ex vivo and in vivo acute preparations,” *J. Neurosci. Methods*, vol. 341, 2020, doi: 10.1016/j.jneumeth.2020.108755.

[27] J. P. Newman *et al.*, “Twister3: a simple and fast microwire twister,” *J. Neural Eng.*, 2020, doi: 10.1088/1741-2552/ab77fa.

[28] J. A. Gorski, T. Talley, M. Qiu, L. Puelles, J. L. R. Rubenstein, and K. R. Jones, “Cortical excitatory neurons and glia, but not GABAergic neurons, are produced in the Emx1-expressing lineage,” *J. Neurosci.*, vol. 22, no. 15, pp. 6309–6314, 2002, doi: 10.1523/jneurosci.22-15-06309.2002.

[29] L. Madisen *et al.*, “A toolbox of Cre-dependent optogenetic transgenic mice for light-induced activation and silencing,” *Nat. Neurosci.*, vol. 15, no. 5, pp. 793–802, 2012, doi: 10.1038/nn.3078.

[30] J. H. Siegle, A. C. López, Y. A. Patel, K. Abramov, S. Ohayon, and J. Voigts, “Open Ephys: An open-source, plugin-based platform for multichannel electrophysiology,” *J. Neural Eng.*, vol. 14, no. 4, 2017, doi: 10.1088/1741-2552/aa5eea.

[31] A. Novais *et al.*, “Hybrid multisite silicon neural probe with integrated flexible connector for interchangeable packaging,” *Sensors*, vol. 21, no. 8, 2021, doi: 10.3390/s21082605.

[32] M. HajjHassan, V. Chodavarapu, and S. Musallam, “NeuroMEMS: Neural probe microtechnologies,” *Sensors*. 2008. doi: 10.3390/s8106704.

[33] N. Grossman, K. Nikolic, C. Toumazou, and P. Degenaar, “Modeling study of the light stimulation of a neuron cell with channelrhodopsin-2 mutants,” *IEEE Trans. Biomed. Eng.*, 2011, doi: 10.1109/TBME.2011.2114883.

[34] J. Shen *et al.*, “Double-Sided Sapphire Optrodes with Conductive Shielding Layers to Reduce Optogenetic Stimulation Artifacts,” *Micromachines*, 2022, doi: 10.3390/mi13111836.

[35] N. McAlinden *et al.*, “Thermal and optical characterization of micro-LED probes for in vivo optogenetic neural stimulation,” *Opt. Lett.*, 2013, doi: 10.1364/ol.38.000992.

[36] H. Yasunaga *et al.*, “MicroLED neural probe for effective in vivo optogenetic stimulation,” *Opt. Express*, 2022, doi: 10.1364/oe.470318.

[37] H. K. Sung, H. K. Lee, C. Wang, and N. Y. Kim, “Design and fabrication of implantable neural probes with monolithically integrated light-emitting diodes for optogenetic applications,” *J. Nanosci. Nanotechnol.*, 2017, doi: 10.1166/jnn.2017.13071.

FIGURES

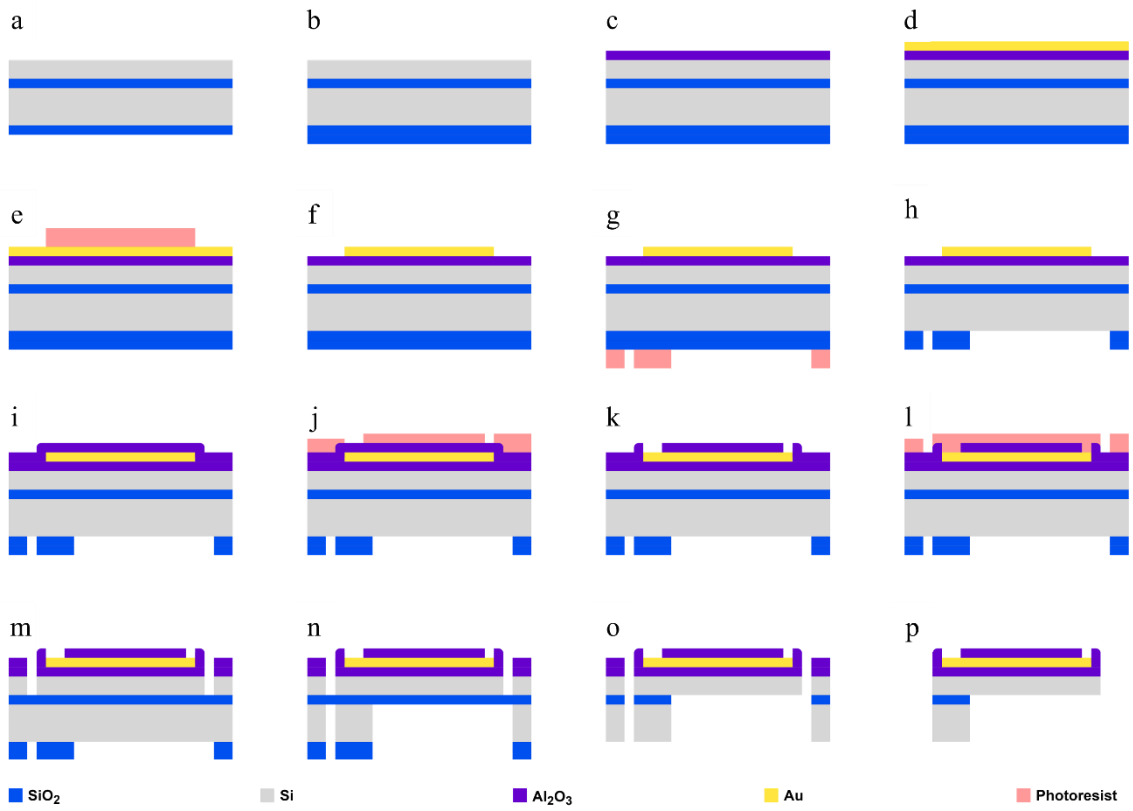

Figure 1. Neural probe fabrication process. (a) Silicon-on-insulator (SOI) wafer. (b) Back-side silicon oxide (SiO_2) layer deposition. (c) Top-side alumina (Al_2O_3) layer deposition. (d-f) Gold (Au) deposition and patterning of interconnect lines and bonding pads. (g-h) Back-side SiO_2 patterning. (i-k). Al_2O_3 passivation and patterning of bonding and conector pads. (l-m) Top-side etching to define probe layout. (m-n) Backside etching. (o-p) Release of device layer. NB: not to scale.

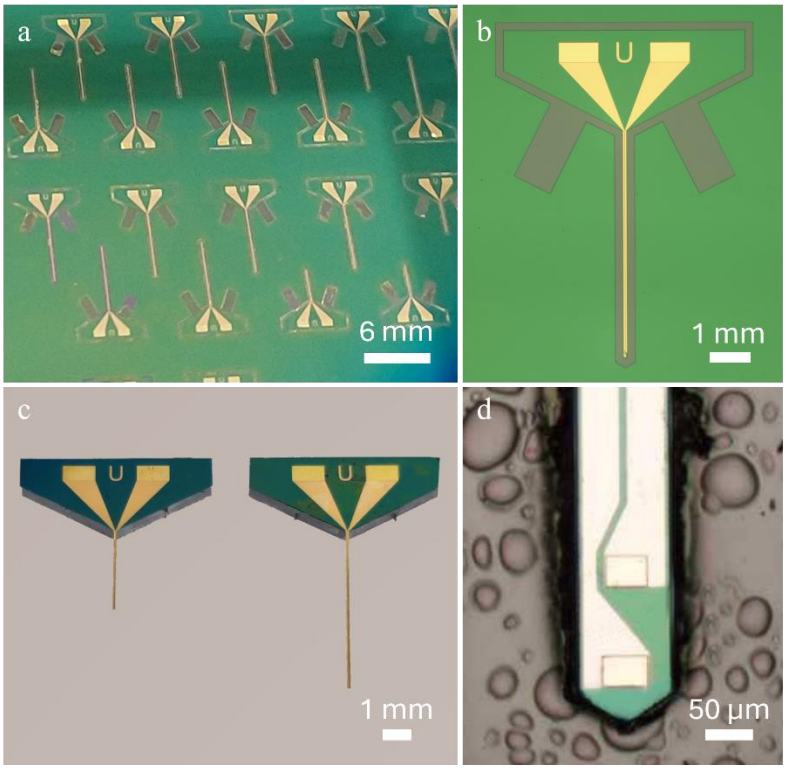

Figure 2. Fabricated neural probes. (a) Detail of SOI wafer with neural probes during the fabrication process. (b) Optical microscopy photograph of neural probe on wafer. (c) Two neural probes released from the wafer, with 3 and 6 mm implantable shanks (left and right, respectively), ready for the µLED integration process. (d) Optical microscopy photograph of neural probe shank's tip on wafer before the final backside etch for release, showing the wide interconnect lines and the two bonding pads for µLED mounting.

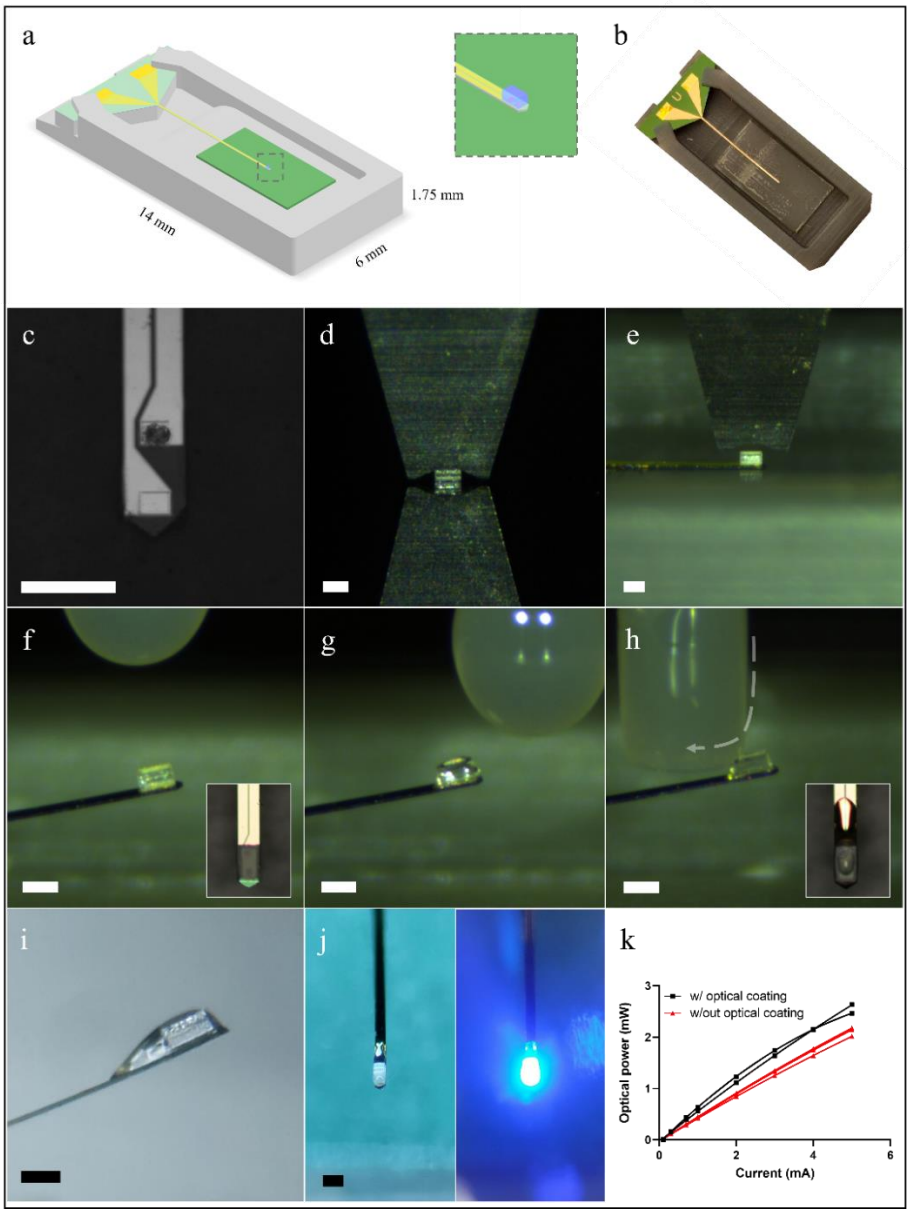

Figure 3. µLED integration on neural probe. (a) Schematic of custom 3D-printed probe holder with an inserted probe. The green patch under the probe's shank corresponds to the termal release tape (TRT). (Inset) Close-up schematic of a bonded µLED in the shank's tip. (b) Photograph of a 6 mm neural probe on a 3D-printed holder with TRT. (c) Shank's tip with the top bonding pad covered in conductive glue for posterior µLED mounting. (d) µLED picking process using the vacuum tip. (e) µLED placement on the shank's tip supported by the TRT on the probe holder. (f) Neural probe shank with bonded µLED, released from the TRT after curing. (Inset) Optical microscopy photograph with top view of the µLED in the probe after curing. (g) µLED after coating with the optical coating applied with the custom 3D-printed tool. (h) Wiping excess optical coating of the µLED's top. White arrow denotes the tip's movement direction. (Inset) Optical microscopy photograph with top view of the µLED after the wiping process. (i) µLED profile photograph after the integration process. The optical coating creates a tail extending away from the tip that smoothens the probe tip topography. (j) Photograph with top view of the finalized probe in an OFF (left) and ON state (right). (k) Measured optical power output of µLEDs with (black lines) and without (red lines) optical coating. Scale in (c),(d),(e),(f),(h),(i) and (j) is 150 µm.

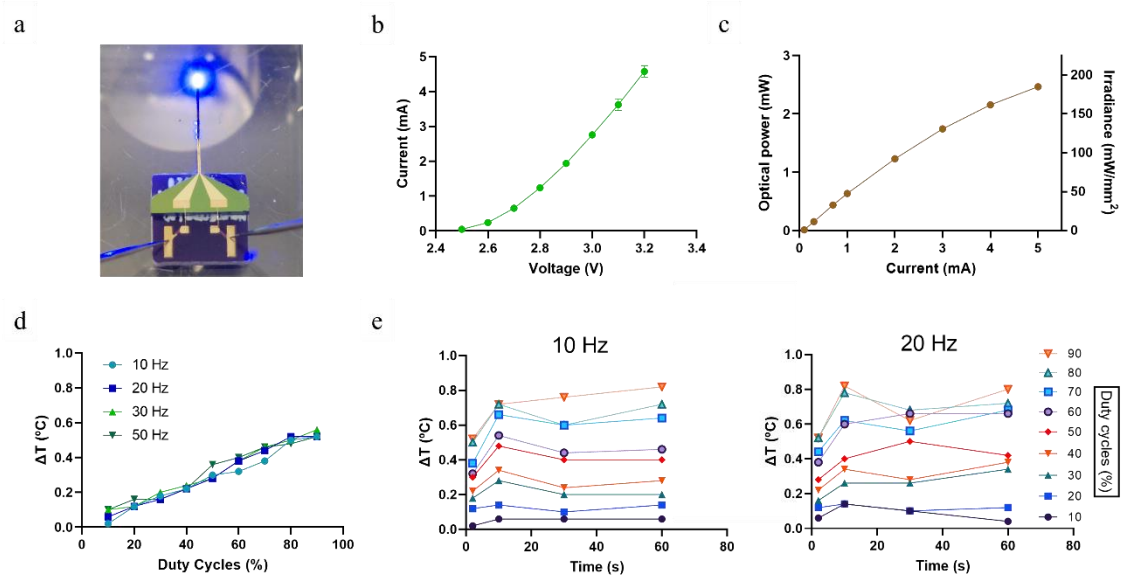

Figure 4. Opto-electrical and thermal characterization of neural probes with µLED. (a) Photograph of probe wire-bonded to the PCB and driven by tungsten needles from probe station. (b) Representative I-V curve with average values from measurements taken from 4 neural probes (error bars are s.e.m). (c) Representative optical power and irradiance of neural probe with µLED as a function of driving current. (d) µLED hotspot temperature elevation for different stimulation frequencies (10, 20, 30 and 50 Hz) and duty cycles (10-90%), at maximum driving current of 5 mA. (e) Temporal dynamics of µLED hotspot temperature elevation for 10 Hz (left) and 20 Hz (right) stimulation at different duty cycles (10-90%), at maximum driving current of 5 mA.

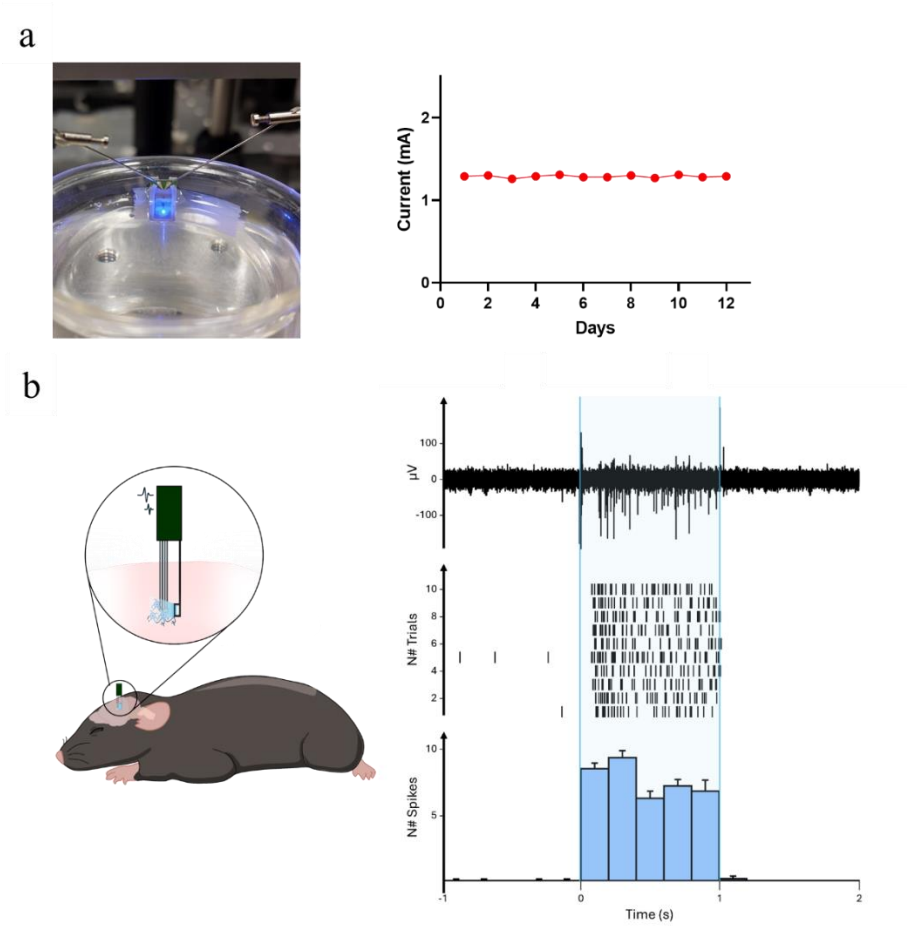

Figure 5. Passivation and in vivo testing. (a) Neural probe submerged in phosphate-buffered saline (PBS) with needles from probe station driving µLED to emit light (left). Current measured daily at 2.8 V during 12 days of continuous immersion in PBS (right). (b) Cartoon of tetrode device and neural probe with µLED assembly implanted in mouse's motor cortex (M1) for simultaneous electrophysiological recordings and optical stimulation (left). Raw trace of one optical stimulation trial with eletrophysiological activity before, during and after optical stimulation (righ, top). Raster plot of spikes detected on 10 optical stimulation trials (right, center). Cummulative peri-stimulus time histogram (PSTH) with total spike count across all optical stimulation trials (right, bottom). Blue shaded area corresponds to optical stimulation period. Bins in PSTH are 200 ms.

TABLES

Table 1. Comparison of different implantable neural probes with µLEDs for brain optogenetics

µLED	µLED dimensions (w x l x h) (µm)	µLED emission peak (nm)	Probe shank dimensions (w x h) (µm)	Cross-sectional area (mm^2)	µLEDs per shank	Probe substrate	Peak working current (mA)	Optical power (mW)	Irrandiance at peak working current (mW/mm^2)	Peak Wall-plug efficiency (%)	Temperature below 1 ºC	In vivo testing	Ref
Commercial flip chip LED	89 x 150 x 80	465	99 x 105	0.014	1	Si	5	2.35	175	14.7	duty cycles below 90% (up to 50 Hz)	Mice, cortex M1	This work
GaN-Si	10 x 15 x 0.5	460	70 x 30	0.0021	3	Si	0.013	0.0003	5	0.8	All parameters if voltage below 3.4 V	Mice, hippocampus CA1	[13]
GaN-Si	25 (diameter)	450	100 x 40	0.0040	16	Si	5	0.2	400	0.8	Duty cycle below 10%	Mice, cortex	[14]
GaN-Si	310 x 41	450	220 x 100	0.022	3	Si	3.5	0.06	1	0.4	-	-	[37]
GaN-Si	22 x 22 x 5	445	800 x 15	0.012	32	Parylene C	0.0085	0.0013	-	0.5	Max 5 ms pulse	-	[15]
GaN-Si	50 (diameter)	460	300 x 300	0.090	5	Si	1	-	15	1	Below 1 mA currents	Mice, hippocampus	[36]
GaN-Sa transferred to PI	50 x 50 x 6.45	-	300 x 20	0.0060	4	PI	-	-	40	1.5	Below 20 Hz	Mice, VTA	[18]
GaN-Sa transferred to PI	125 x 180	480 / 630	320 x 120	0.038	1	PI	3 / 10	-	60 / 45	8.0 / 4.0	Currents below 3 mA / Below 30 Hz up to 10 mA	Mice, VTA	[19]
GaN-Sa transferred to Si	100 (diameter)	455	150 x 65	-	10	Si	5	0.450	56	2.0	Currents below 3 mA and pulses below 500 ms	Mice, cortex S1	[17]
GaN-Sa	250 x 490	444	400 x 200	0.080	1	Sa	35	-	5	-	-	-	[34]
GaN-Sa	40 (diameter)	450	80 x 101	0.0081	5	Sa	0.1	-	10	-	Below 50 Hz	-	[35]
Commercial flip chip LED	220 x 270 x 50	470	350 x 130	0.045	1	PI	5	-	50	-	Below 60% duty cycle	Mic, Nac / VTA	[21]
Commercial flip chip LED	220 x 270 x 50	460	250 x 60	0.016	3	PI	10	0.5	10	1.7	-	Mice, nRT	[23]
Commercial flip chip LED	220 x 270 x 50	465 / 540	650 x 700	0.45	2	PDMS	-	-	12	-	Duty cycles below 70%	Mice, Nac	[20]
Commercial flip chip LED	290 x 550 x 100	455	900 x 500	0.45	1	PCD	-	-	1.55	-	Below 1 Hz and 100 ms pulses	Rat, V1	[22]